# Journal of Materials Chemistry A



## COMMUNICATION



Cite this: *J. Mater. Chem. A*, 2020, **8**, 1646

Received 26th November 2019 Accepted 3rd January 2020

DOI: 10.1039/c9ta12937e

rsc.li/materials-a

# Synthesis and Li-ion electrode properties of layered MAB phases $Ni_{n+1}ZnB_n$ (n=1, 2)†

Amir A. Rezaie, <sup>©</sup> <sup>ac</sup> Zheng Yan, <sup>b</sup> Jan P. Scheifers, <sup>©</sup> <sup>a</sup> Jian Zhang, <sup>©</sup> <sup>c</sup> Juchen Guo <sup>©</sup> \* <sup>bc</sup> and Boniface P. T. Fokwa <sup>©</sup> \* <sup>ac</sup>

Ternary MAB phases (layered transition metal borides) have recently attracted interest due to their exfoliation potential toward MBenes (analogous to MXenes), which are predicted to have excellent Li-ion battery performance. We have achieved single-phase synthesis of two MAB phases with general composition  $Ni_{n+1}ZnB_n$  (n = 1, 2), the crystal structures of which contain zinc layers sandwiched between thin (n = 1) and thick (n = 2) Ni-B slabs. Highly stacked MAB sheets were confirmed by X-ray diffraction and high-resolution scanning electron microscopy for both materials. Exposing  $Ni_{n+1}ZnB_n$  to diluted hydrochloric acid led to the creation of crystalline microporous structures for n = 1 and non-porous detached sheets for n = 2. Both morphologies transformed the inactive bulk materials into highly active Li-ion battery anodes with capacities of  $\sim$ 90 mA h g<sup>-1</sup> (n = 1) and  $\sim$ 70 mA h g<sup>-1</sup> (n = 2) at a 100 mA g<sup>-1</sup> lithiation–delithiation rate. The XPS analysis and BET surface area measurements reveal that the increased surface area and the reversible redox reaction of oxidized nickel species are responsible for this drastic increase of the lithiationdelithiation capacity. This proof of concept opens new avenues for the development of porous MAB, MAB nanosheets, MBenes and their composites for metal-ion battery applications.

Since the discovery of MAX phases, these layered transition metal carbides (X = C) and nitrides (X = N) with general formula  $M_{n+1}AX_n$  (n=1–3) have gained interest among scientists due to their mixed metallic and ceramic properties.<sup>1-3</sup> These properties include machinability, high corrosion resistance, high ductility, excellent electrical and thermal conductivity, thermal shock resistance,  $etc^{4-7}$ . In 2011 Gogotsi et al.<sup>8</sup> introduced MXenes (M = early transition metal, X = C or N),

which are derived from the MAX phases by chemical etching of the A layer, as promising candidates for lithium-ion battery anodes.9-11 MXenes have been considered for other applications such as batteries, 9-11 supercapacitors, 9,12 and magnetic shielding13 etc. In 2015, Hillebrecht et al.14 introduced a MAX-related family of layered materials called MAB phases - MAX phases with X = boron. Even though these MAB phases are chemically and structurally different from the MAX phases, they have similar properties such as high conductivity,15 stiffness15 and resistant to thermal shock.16 MAB phases include compounds with different compositions and structures such as M2AlB2 (Cmmm), 14 MoAlB (Cmcm), 17 Cr<sub>3</sub>AlB<sub>4</sub> (Immm), 14 Ru<sub>2</sub>ZnB<sub>2</sub> (I4<sub>1</sub>/ amd), 18 Y<sub>2</sub>SiB<sub>8</sub> (P4/mbm), 19 Cr<sub>5</sub>SiB<sub>3</sub>, 16 and Ni<sub>3</sub>ZnB<sub>2</sub> (C2/m). 20-23 The variety of MAB structures differentiate them from the MAX phases which are mainly hexagonal (space group  $P6_3/mmc$ ). This significant structural difference is directed by the boron substructure which varies from dumbbell, to zigzag B<sub>4</sub> fragment, to zigzag boron chain, to chain of boron hexagons and chain of boron double hexagons.14 In MAX phases, however, no bond exists between X (C, N) atoms. In addition, significant bonding interactions exist between boron and the A atoms in MAB structures, while no significant interaction exist between X and A in MAX structures.24 These significant A-B interactions are likely the main reason why A is rather difficult to be etched out of the MAB structures to produce MBenes, 25-27 while the absence of A-X interactions in MAX phases supports the easy exfoliation.24 This analysis shows that exfoliating Ni<sub>n+1</sub>ZnB<sub>n</sub> phases will be as difficult as the other MAB phases. Although no MBene has been realized quantitatively yet, theory has suggested that these materials have great potential in battery and electrocatalysis applications.28 Even though several binary transition metal borides such as VB2 and TiB2 have been investigated as anodes for non-rechargeable battery systems, 29,30 the electrochemical properties of MAB phases for rechargeable battery electrodes has not been experimentally investigated, to best of our knowledge.

The structural diversity of MAB phases give them a unique and untapped advantage: many of them contain M transition

<sup>&</sup>lt;sup>a</sup>Department of Chemistry, University of California, Riverside, 92521 Riverside, CA, USA. E-mail: bfokwa@ucr.edu

<sup>&</sup>lt;sup>b</sup>Department of Chemical and Environment Engineering, University of California, Riverside, 92521 Riverside, CA, USA. E-mail: jguo@engr.ucr.edu

<sup>&</sup>lt;sup>c</sup>Materials Science and Engineering Program, University of California, Riverside, 92521 Riverside, CA, USA

<sup>†</sup> Electronic supplementary information (ESI) available. See DOI: 10.1039/c9ta12937e

elements<sup>14</sup> that are important for Li-ion battery performance: Ti, V, Cr, Fe, Mn and Ni.31,32 In this study, we will focus on Ni<sub>2</sub>ZnB and Ni<sub>3</sub>ZnB<sub>2</sub>, which are evaluated for the first time for their Li-ion electrode properties as a proof of concept. We show that the bulk samples are largely inactive as battery materials, however, exposing Ni<sub>2</sub>ZnB and Ni<sub>3</sub>ZnB<sub>2</sub> to an acid treatment leads to two unexpected morphological changes that drastically increase their Li-ion battery performance.

The Ni-Zn-B system was previously investigated at 800 °C by Malik et al. showing the existence of different phases such as Ni<sub>12</sub>ZnB<sub>8</sub> (space group: Cmca), Ni<sub>21</sub>Zn<sub>2</sub>B<sub>20</sub> (space group: Cmca), Ni<sub>3</sub>ZnB<sub>2</sub> (space group: C2/m), Ni<sub>2</sub>ZnB (space group: C2/m), and  $Ni_3Zn_2B$  (space group: C2/m). <sup>20–23,33</sup> Out of all these phases, only Ni<sub>2</sub>ZnB and Ni<sub>3</sub>ZnB<sub>2</sub> have layered structures<sup>20,21</sup> with a general chemical composition  $(Ni_{n+1}ZnB_n)$  like the MAX phases  $(M_{n+1}AX_n)$ . In these two layered MAB structures, beside the expected Ni-Zn and Ni-B bonding interactions, Zn and B atoms also significantly interact leading to wave-like arrangement of the zinc layer in both structures (Fig. 1, left).

The synthesis of phases in the Ni-Zn-B system is quite challenging: as the Ni-Zn-B isotherm at 800 °C (ref. 20) suggests (Fig. S1†) Ni<sub>2</sub>ZnB and Ni<sub>3</sub>ZnB<sub>2</sub> are stable at this temperature. However, due to their small phase areas in the isotherm, a small shift in the composition will lead to the formation of impurities based on the scalene triangles representing a three-phase equilibrium. For example, in their recent discovery of Ni<sub>2</sub>ZnB Rogl et al. obtained a multiphase product (Ni<sub>2</sub>ZnB, Ni<sub>3</sub>Zn<sub>2</sub>B, Ni<sub>2</sub>Zn<sub>11</sub>).<sup>20</sup> The same authors previously synthesized single-phase Ni<sub>3</sub>ZnB<sub>2</sub> by mixing NiB<sub>x</sub> master alloy with fine Zn filings in proper compositional ratio. The mixture

was then submitted to several preparation steps (milled/coldpressed/heat-treated/annealed/quenched/re-milled/hotpressed) that enabled the synthesis of a polycrystalline sample with isotropic particles (no preferred orientation observed).23 We have developed a new approach in our synthesis, by first preparing a high quality Ni<sub>2</sub>B master alloy through arc-melting as it melts congruently (Fig. S2†). Ni<sub>2</sub>B was then powdered and mixed with the remaining elements according to the targeted composition, pressed to a pellet and submitted to a meltingsolidification technique including pre-alloying and heat treatments with regrinding steps (see the detailed procedure given in the ESI and the temperature profiles in Fig. S3†). This synthesis method led to the formation of highly anisotropic particles of Ni<sub>2</sub>ZnB and Ni<sub>3</sub>ZnB<sub>2</sub>, as proven by the following analysis. Rietveld refinements (Fig. 1) of the powder X-ray diffraction (PXRD) patterns were conducted on both products. Severe intensity mismatches (Fig. S4†) were initially observed mainly for the 00l reflections, but they were successfully corrected using preferred orientation refinement along the c-axis, hinting at layered morphologies of the two samples. Indeed, high-resolution scanning electron microscopy (HRSEM) images of the bulk Ni<sub>2</sub>ZnB and Ni<sub>3</sub>ZnB<sub>2</sub> products showed highly stacked thin sheets (Fig. 2a and b and S5†). The PXRD refinement results confirmed the expected crystal structures and no impurity peaks were detected, hinting at almost single-phase syntheses, but SEM backscattering imaging detected small Ni-rich impurity inclusions in the samples (see Fig. S6†). Energy dispersive X-

ray spectroscopy (EDS) through elemental mapping confirmed

the presence of all elements and their homogeneous distribu-

tion in both samples (Fig. S5 and S6†). Inductively coupled

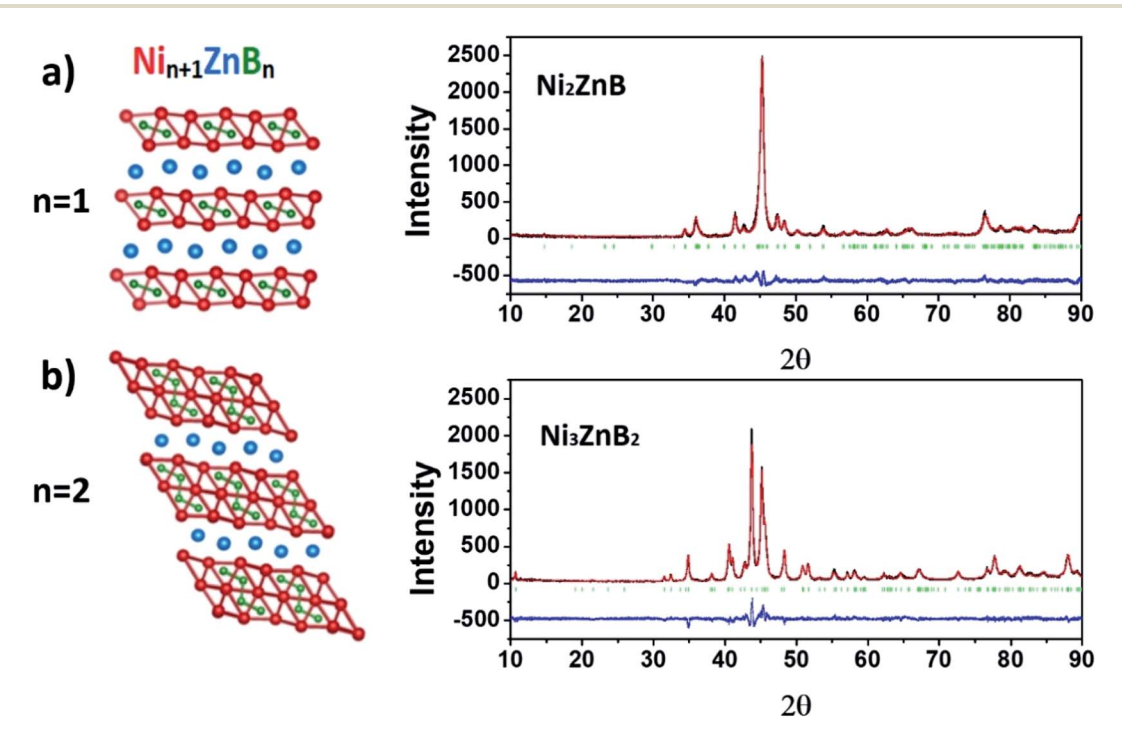


Fig. 1 Crystal structures and Rietveld refinements of the powder XRD patterns of Ni<sub>2</sub>ZnB (a) and Ni<sub>3</sub>ZnB<sub>2</sub> (b). The red and the black curves represent the measured and the calculated patterns, respectively, whereas the blue curves show the intensity difference. The positions of the Bragg peaks are shown in green.

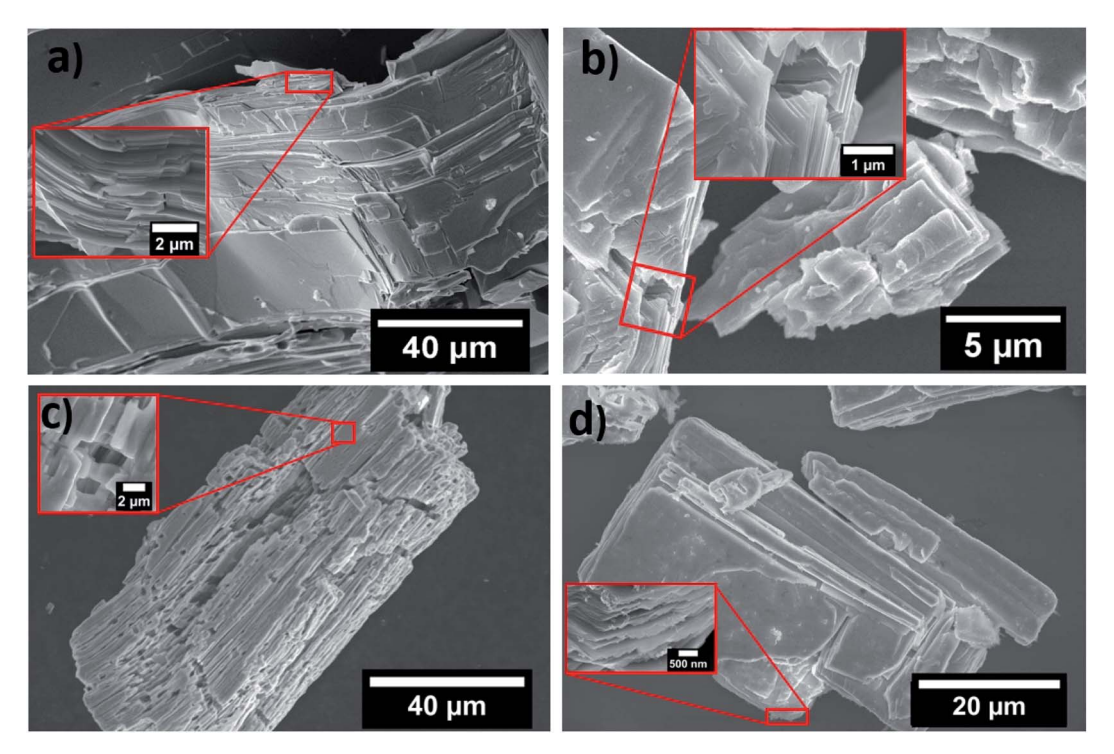


Fig. 2 SEM images of the as-synthesized (a and b) and the 72 h HCl-etched (c and d) samples of Ni<sub>2</sub>ZnB (a and c) and Ni<sub>3</sub>ZnB<sub>2</sub> (b and d).

plasma (ICP) spectroscopy measurements provided a Ni: Zn ratio of 3.16:1 and 2.20:1 for  $Ni_3ZnB_2$  and  $Ni_2ZnB$ , respectively. The slight deviation of the ICP results from the ideal Ni: Zn ratios is likely due to the Ni-rich impurity inclusions mentioned above. Furthermore, selected area electron diffraction (SAED) from a transmission electron microscopy (TEM) image of a  $Ni_3ZnB_2$  thin particle confirmed its crystallinity with diffraction peaks indexed according to its crystal structure (space group C2/m, Fig. S7†).

To investigate the possible Zn etching from  $Ni_2ZnB$  and  $Ni_3ZnB_2$  bulk samples, several etchants (HCl, NaOH and FeCl $_3$ /HCl) were tried (see ESI for details†). We found that only 1 M HCl had the most promising results. The  $Ni_2ZnB$  and  $Ni_3ZnB_2$  bulk samples were powdered and treated with 1 M HCl acid for 72 hours. The prepared solutions were regularly shaken and ultrasonicated every 8 hours for about 3 minutes. Ultrasonication broke the bulk crystals into small pieces thereby accelerating the acid etching. After 72 hours, most of the sample

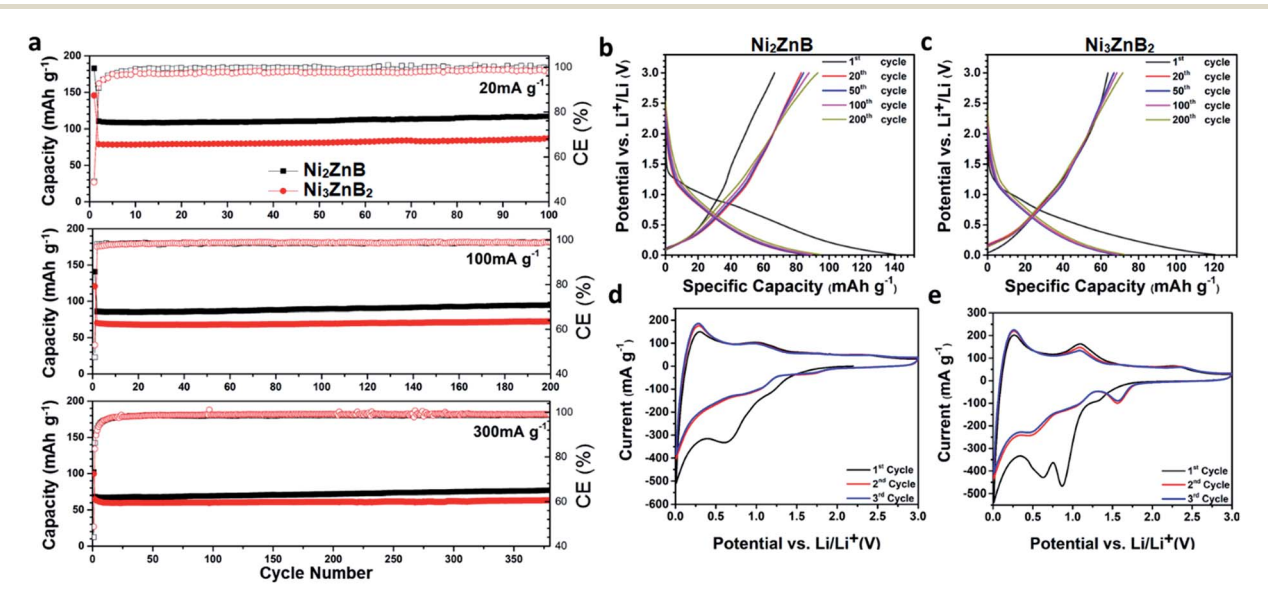


Fig. 3 Electrochemical characterizations of  $Ni_2ZnB$  and  $Ni_3ZnB_2$  electrodes. (a) Cycle stability of  $Ni_2ZnB$  and  $Ni_3ZnB_2$  at various current rates; representative lithiation and delithiation curves of (b)  $Ni_2ZnB$  and (c)  $Ni_3ZnB_2$  at the rate of 100 mA  $g^{-1}$ ; cyclic voltammetry of (d)  $Ni_2ZnB$  and (e)  $Ni_3ZnB_2$  at 1 mV  $s^{-1}$  scan rate from 0.01 to 3.0 V vs.  $Li/Li^+$ .

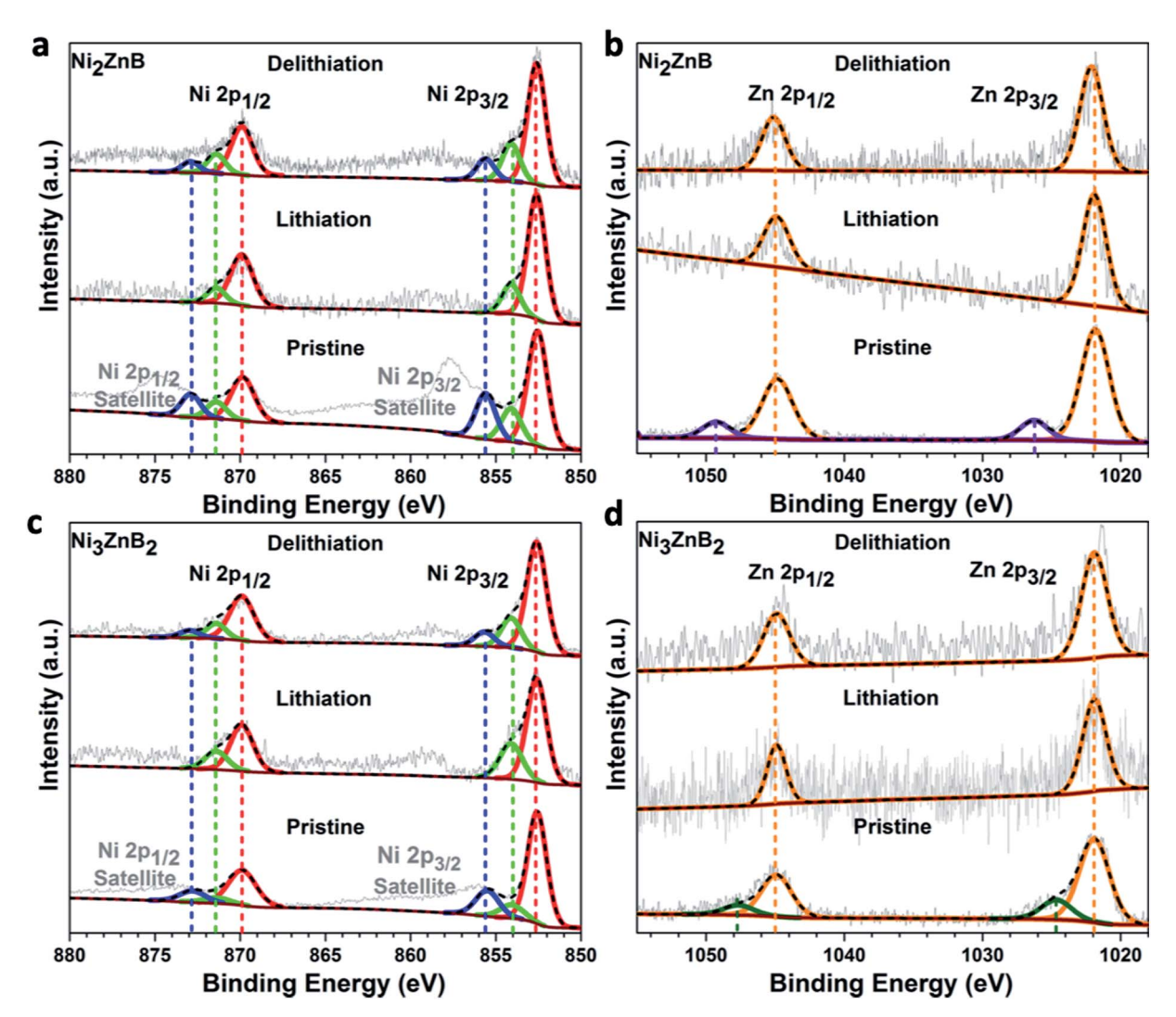


Fig. 4 XPS Ni 2p and Zn 2p spectra of Ni<sub>2</sub>ZnB (a and b) and Ni<sub>3</sub>ZnB<sub>2</sub> (c and d) after acid etching (pristine) and after the first lithiation—delithiation cycle.

had precipitated, leaving an almost colorless solution, an indication that a complete Zn removal, as observed in the case of Al etching in MAX phases such as  $Ti_{n+1}AlC_n$ , has not occurred. Instead, very small amounts of etched materials were obtained, and our preliminary analysis suggests that they contain less Zn than the bulk and the precipitated samples, thereby hinting at only partial etching (results to be communicated elsewhere), as observed in recent etching studies on Al-based MAB phases.26,27,34 The acid-treated Ni2ZnB and Ni3ZnB2 precipitates were investigated by PXRD, SEM, EDS, and ICP. According to PXRD, the Ni<sub>2</sub>ZnB and Ni<sub>3</sub>ZnB<sub>2</sub> samples remained crystalline and their crystal structures did not change during the etching process (Fig. S8†). However, their morphologies were affected, as shown by SEM images in Fig. 2c and d: SEM analysis of the etched Ni<sub>2</sub>ZnB crystals shows that the top sheets were attacked by HCl leading to the emergence of pores and layer openings (Fig. 2c and S9†). The pore sizes ranged from 100 nanometers to a few micrometers. The SEM analysis of etched Ni<sub>3</sub>ZnB<sub>2</sub> crystals indicated that the top sheets were not attacked by the acid, as

only the layer openings were observed (Fig. 2d). This finding reveals that Ni<sub>3</sub>ZnB<sub>2</sub> has more robust layers than Ni<sub>2</sub>ZnB, which may be due to the thickness differences of the Ni-B slabs (Fig. 1, left). Since our chemical analysis (see ESI†) showed the same composition between these precipitates and the unetched samples, we hypothesize that the layer opening observed after etching is due to the ultrasonication. We are currently carrying out further ultrasonication experiments in different solutions to verify this hypothesis.

The BET surface areas of etched Ni<sub>2</sub>ZnB and Ni<sub>3</sub>ZnB<sub>2</sub> are 95.9 m<sup>2</sup> g<sup>-1</sup> and 0.7 m<sup>2</sup> g<sup>-1</sup>, respectively. The pristine materials did not produce meaningful BET values, with the best measurement leading to a negligible value of 0.03 m<sup>2</sup> g<sup>-1</sup>, indicating orders of magnitude improvement of the surface area after the acid treatment. After etching, the newly exposed surfaces are believed to be terminated by hydroxide or oxide groups like in MXenes.9-12 These surface species are capable of reversible redox reactions, thus interesting electrochemical properties relevant to battery materials can be expected. We have therefore examined the etched MAB phases in Li-ion half-cells using Li foil as the counter electrode. The MAB electrode was composed of 80 wt% of Ni<sub>2</sub>ZnB (or Ni<sub>3</sub>ZnB<sub>2</sub>), 10 wt% of polyvinylidene difluoride (PVDF) as binder, and 10 wt% of acetylene black as the conductive additive. Fig. 3a shows the cycle stability and coulombic efficiency (CE) under various lithiation-delithiation rates of 20 mA  $g^{-1}$ , 100 mA  $g^{-1}$  and 300 mA  $g^{-1}$ . At 20 mA  $g^{-1}$ , the first lithiation capacity of Ni<sub>2</sub>ZnB electrode was approximately 180 mA h  $g^{-1}$  and a reversible capacity of  $\sim$ 110 mA h  $g^{-1}$ was achieved. At higher rates, the reversible capacities were  $\sim$ 90 mA h g<sup>-1</sup> at 100 mA g<sup>-1</sup> and  $\sim$ 70 mA h g<sup>-1</sup> at 300 mA g<sup>-1</sup>. The first cycle coulombic efficiency (CE) was 49.2% at 20 mA g<sup>-1</sup>, and the CE in the following cycles improved fast to an average value of 99.3%. In all the specific capacity measurements, Ni<sub>2</sub>ZnB demonstrated a 20 mA h g<sup>-1</sup> (at 100 mA g<sup>-1</sup>) higher specific capacity than Ni<sub>3</sub>ZnB<sub>2</sub> (Fig. 3a, middle), which is likely due to the higher surface area of etched Ni<sub>2</sub>ZnB. Both materials demonstrate excellent cycle stability with a slight incremental trend of capacity, which most probably results from accessibility of Li ions to active sites that has improved upon cycling.35 The powder XRD analysis of the MAB phases after the first lithiation and delithiation (Fig. S8†) shows that the crystal structures of Ni<sub>2</sub>ZnB and Ni<sub>3</sub>ZnB<sub>2</sub> are retained. However, the intensity of the peaks significantly decreased, indicating that the crystallinity is reduced in these materials upon electrochemical reaction with Li. The representative lithiation-delithiation potential curves and cyclic voltammograms (CV) are shown in Fig. 3(b-e), and both methods indicate significant irreversibility in the first cycle (leading to low initial CE), a behavior also reported for similar materials such as MXenes and their composites. 9,10 To understand the origin of the irreversible capacity, the oxidation states of the surface elements were analyzed by X-ray photoelectron spectroscopy (XPS) after the acid etching, the first lithiation, and the first delithiation. As shown in Fig. 4a, the Ni species on the surface of Ni<sub>2</sub>ZnB after etching include metallic Ni (Ni 2p<sub>3/2</sub> at 852.6 eV),  $Ni^{2+}$  (Ni  $2p_{3/2}$  at 854.0 eV), and  $Ni^{3+}$  (Ni  $2p_{3/2}$  at 855.6 eV). After the first lithiation the Ni<sup>3+</sup> species was completely reduced to lower oxidation state. The Ni<sup>2+</sup> species was also significantly reduced (using the peak of metallic Ni as the standard). After the delithiation, Ni<sup>3+</sup> species re-emerged, however, the lower peak intensity relative to the etched sample indicates that the redox reaction of nickel is not completely reversible in the first cycle. The Zn species (Fig. 4b) on the surface of etched Ni<sub>2</sub>ZnB show two states including metallic Zn (Zn 2p<sub>3/2</sub> at 1021.9 eV) and an oxidized state (Zn 2p<sub>3/2</sub> at 1026.3 eV). After the first lithiation, the oxidized Zn is completely reduced to the metallic state, and this reduction process is irreversible indicated by the XPS Zn 2p spectrum after the delithiation. As displayed in Fig. 4c and d, the Ni and Zn surface species on Ni<sub>3</sub>ZnB<sub>2</sub> show the same behavior as observed in Ni<sub>2</sub>ZnB. The surface boron species in both compounds are inert as indicated by their XPS B 1s spectra (Fig. S10†). Therefore, we suggest that the electrochemical redox reactions of Ni species on the surface contribute to the electrochemical performance of these two MAB phases. The irreversible reduction of Ni and Zn species in the first cycle is a major cause for the low initial CE in addition to the possible side reactions of solid electrolyte interphase formation.

#### Conclusions

In this study, the syntheses of the MAB phases  $Ni_{n+1}ZnB_n$  (n = 1, 2) were systematically investigated. The synthesized MAB phases were exposed to dilute HCl in order to study the effect of etching on their crystal structure. It was seen that the proposed MAB phases get partially attacked by the acid and form pores and sheet openings. The battery performances of the unetched and etched MAB phases were investigated. While the bulk Ni<sub>2</sub>ZnB and Ni<sub>3</sub>ZnB<sub>2</sub> were not active, the etched phases showed a capacity of  $\sim$ 90 mA h g<sup>-1</sup> and  $\sim$ 75 mA h g<sup>-1</sup>, respectively. XPS and BET analyses suggest that increased surface area and electrochemical redox reactions of surface Ni species are responsible for the drastic change in battery performances. Future works should focus on increasing the surface area of these and other MAB phases containing elements that can undergo redox reactions toward applications in various metalion batteries.

#### Conflicts of interest

There are no conflicts to declare.

### Acknowledgements

This work was supported by the startup fund to BPTF at UC Riverside and the National Science Foundation Career award to BPTF (no. DMR-1654780). The CFAMM center at UC Riverside for electron microscopy and microanalysis.

#### References

- 1 M. Barsoum and T. El-Raghy, Synthesis and characterization of a remarkable ceramic: Ti<sub>3</sub>SiC<sub>2</sub>, *J. Am. Ceram. Soc.*, 1996, **79**(7), 1953–1956.
- 2 W. Jeitschko, H. Nowotny and F. Benesovsky, Carbides of formula T<sub>2</sub>MC, *J. Less-Common Met.*, 1964, 7(2), 133–138.
- 3 J. Schuster, H. Nowotny and C. Vaccaro, The ternary systems: CrAlC, VAlC, and TiAlC and the behavior of H-phases (M<sub>2</sub>AlC), *J. Solid State Chem.*, 1980, 32(2), 213–219.
- 4 M. W. Barsoum and T. El-Raghy, The MAX phases: unique new carbide and nitride materials: ternary ceramics turn out to be surprisingly soft and machinable, yet also heat-tolerant, strong and lightweight, *Am. Sci.*, 2001, **89**(4), 334–343.
- 5 M. Khazaei, M. Arai, T. Sasaki, M. Estili and Y. Sakka, Trends in electronic structures and structural properties of MAX phases: a first-principles study on M<sub>2</sub>AlC (M = Sc, Ti, Cr, Zr, Nb, Mo, Hf, or Ta), M<sub>2</sub>AlN, and hypothetical M<sub>2</sub>AlB phases, *J. Phys.: Condens. Matter*, 2014, **26**(50), 505503.
- 6 M. Barsoum, T. El-Raghy and M. Ali, Processing and characterization of Ti<sub>2</sub>AlC, Ti<sub>2</sub>AlN, and Ti<sub>2</sub>AlC<sub>0.5</sub>N <sub>0.5</sub>, *Metall. Mater. Trans. A*, 2000, **31**(7), 1857–1865.

- 7 M. Barsoum and T. El-Raghy, Room-temperature ductile carbides, Metall. Mater. Trans. A, 1999, 30(2), 363-369.
- 8 M. Naguib, M. Kurtoglu, V. Presser, J. Lu, J. Niu, M. Heon, et al., Two-dimensional nanocrystals produced by exfoliation of Ti<sub>3</sub>AlC<sub>2</sub>, Adv. Mater., 2011, 23(37), 4248-4253.
- 9 M. Q. Zhao, C. E. Ren, Z. Ling, M. R. Lukatskaya, C. Zhang, K. L. Van Aken, et al., Flexible MXene/carbon nanotube composite paper with high volumetric capacitance, Adv. Mater., 2015, 27(2), 339-345.
- 10 M. Naguib, J. Come, B. Dyatkin, V. Presser, P.-L. Taberna, P. Simon, et al., MXene: a promising transition metal carbide anode for lithium-ion batteries, Electrochem. Commun., 2012, 16(1), 61-64.
- 11 X. Liang, A. Garsuch and L. F. Nazar, Sulfur cathodes based on conductive MXene nanosheets for high-performance lithium-sulfur batteries, Angew. Chem., Int. Ed., 2015, **54**(13), 3907–3911.
- 12 M. R. Lukatskaya, O. Mashtalir, C. E. Ren, Y. Dall'Agnese, P. Rozier, P. L. Taberna, et al., Cation intercalation and high volumetric capacitance of two-dimensional titanium carbide, Science, 2013, 341(6153), 1502-1505.
- 13 F. Shahzad, M. Alhabeb, C. B. Hatter, B. Anasori, S. M. Hong, C. M. Koo, et al., Electromagnetic interference shielding with 2D transition metal carbides (MXenes), Science, 2016, 353(6304), 1137-1140.
- 14 M. Ade and H. Hillebrecht, Ternary borides Cr<sub>2</sub>AlB<sub>2</sub>, Cr<sub>3</sub>AlB<sub>4</sub>, and Cr<sub>4</sub>AlB<sub>6</sub>: The first members of the series (CrB<sub>2</sub>) n CrAl with n = 1, 2, 3 and a unifying concept for ternary borides as MAB-phases, Inorg. Chem., 2015, 54(13), 6122-6135.
- 15 Y. Zhou, H. Xiang, F.-Z. Dai and Z. Feng, Electrical conductive and damage-tolerant nanolaminated MAB phases Cr<sub>2</sub>AlB<sub>2</sub>, Cr<sub>3</sub>AlB<sub>4</sub> and Cr<sub>4</sub>AlB<sub>6</sub>, Mater. Res. Lett., 2017, 5(6), 440-448.
- 16 Y. Zhou, H. Xiang, F.-Z. Dai and Z. Feng, Cr<sub>5</sub>Si<sub>3</sub>B and Hf<sub>5</sub>Si<sub>3</sub>B: new MAB phases with anisotropic electrical, mechanical properties and damage tolerance, J. Mater. Sci. Technol., 2018, 34(8), 1441-1448.
- 17 S. Kota, E. Zapata-Solvas, A. Ly, J. Lu, O. Elkassabany, A. Huon, et al., Synthesis and characterization of an alumina forming nanolaminated boride: MoAlB, Sci. Rep., 2016, 6, 26475.
- 18 K. Petry and W. Jung, Ternäre Boride der Rutheniums mit Aluminium und Zink, Z. Kristallogr., 1988, 182, 153.
- 19 Y. Zhou, H. Xiang, F. Z. Dai and Z. Feng, Y<sub>5</sub>Si<sub>2</sub>B<sub>8</sub>: a theoretically predicted new damage-tolerant MAB phase with layered crystal structure, J. Am. Ceram. Soc., 2018, **101**(6), 2459-2470.
- 20 F. Failamani, R. Podloucky, J. Bursik, G. Rogl, H. Michor, H. Müller, et al., Boron-phil and boron-phob structure units in novel borides Ni<sub>3</sub>Zn<sub>2</sub>B and Ni<sub>2</sub>ZnB: experiment and first principles calculations, Dalton Trans., 2018, 47(10), 3303-3320.
- 21 Z. P. Malik, O. Sologub, A. Grytsiv, G. Giester and P. F. Rogl, Crystal Structure of Novel Ni-Zn Borides: First Observation

- of a Boron-Metal Nested Cage Unit: B20Ni6, Inorg. Chem., 2011, 50(16), 7669-7675.
- 22 Z. Malik, A. Grytsiv, P. Rogl, G. Giester and J. Bursik, Phase relations and structural features in the system Ni-Zn-B, J. Solid State Chem., 2013, 198, 150-161.
- 23 Z. Malik, A. Grytsiv, H. Michor, G. Rogl, S. Puchegger, H. Müller, et al., Physical properties of the ternary borides Ni<sub>21</sub>Zn<sub>2</sub>B<sub>20</sub> and Ni<sub>3</sub>ZnB<sub>2</sub>, J. Alloys Compd., 2013, 550, 302-307.
- 24 Z. Guo, L. Zhu, J. Zhou and Z. Sun, Microscopic origin of MXenes derived from layered MAX phases, RSC Adv., 2015, **5**, 25403-25408.
- 25 H. Zhang, H. Xiang, F.-z Dai, Z. Zhang and Y. Zhou, First demonstration of possible two-dimensional MBene CrB derived from MAB phase Cr<sub>2</sub>AlB<sub>2</sub>, J. Mater. Sci. Technol., 2018, 34(11), 2022-2026.
- 26 L. T. Alameda, C. F. Holder, J. L. Fenton and R. E. Schaak, Partial etching of Al from MoAlB single crystals to expose catalytically active basal planes for the hydrogen evolution reaction, Chem. Mater., 2017, 29(21), 8953-8957.
- 27 L. T. Alameda, P. Moradifar, Z. P. Metzger, N. Alem and R. E. Schaak, Topochemical deintercalation of Al from MoAlB: stepwise etching pathway, layered intergrowth structures, and two-dimensional MBene, J. Am. Chem. Soc., 2018, 140(28), 8833-8840.
- 28 Z. Guo, J. Zhou and Z. Sun, New two-dimensional transition metal borides for Li ion batteries and electrocatalysis, J. Mater. Chem. A, 2017, 5(45), 23530-23535.
- 29 J. Stuart, M. Lefler, C. P. Rhodes and S. Licht, High Energy Capacity TiB<sub>2</sub>/VB<sub>2</sub> Composite Metal Boride Air Battery, J. Electrochem. Soc., 2015, 162(3), A432-A436.
- 30 H. Yang, Y. Wang, X. Ai and C. Cha, Metal borides: competitive high capacity anode materials for aqueous primary batteries, Electrochem. Solid-State Lett., 2004, 7(7), A212-A215.
- 31 A. Manthiram, J. C. Knight, S. T. Myung, S. M. Oh and Y. K. Sun, Nickel-rich and lithium-rich lavered oxide cathodes: progress and perspectives, Adv. Energy Mater., 2016, 6(1), 1501010.
- 32 N. Nitta, F. Wu, J. T. Lee and G. Yushin, Li-ion battery materials: present and future, Mater. Today, 2015, 18(5), 252-264.
- 33 S. Bhan and A. Lal, The B-Ni-Zn(Boron-Nickel-Zinc) System, J. Alloy Phase Diagrams, 1990, 6(3), 147-152.
- 34 L. T. Alameda, R. W. Lord, J. A. Barr, P. Moradifar, Z. P. Metzger, B. C. Steimle, et al., Multi-Step Topochemical Pathway to Metastable Mo<sub>2</sub>AlB<sub>2</sub> and Related Two-Dimensional Nanosheet Heterostructures, J. Am. Chem. Soc., 2019, 141, 10852-10861.
- 35 O. Mashtalir, M. R. Lukatskaya, M. Q. Zhao, M. W. Barsoum and Y. Gogotsi, Amine-Assisted Delamination of Nb<sub>2</sub>C MXene for Li-Ion Energy Storage Devices, Adv. Mater., 2015, 27(23), 3501-3506.